Article

Numerical Simulation and Wear Resistance Property of Ni-Based Alloy Coating on the Surface of Ti-6Al-4V Substrate

Yu Liu [1,2,*], Xiaofu Liu [1], Zhiqiang Xu [1,3] and Miao Yu [4]

1   School of Mechanical Engineering, Northeast Electric Power University, Jilin 132012, China; liuxf980824@163.com (X.L.); xiaoxu00521@163.com (Z.X.)
2   International Shipping Research Institute, Gongqing Institute of Science and Technology, Gongqing 332020, China
3   Beijing Electric Power Transmission and Transformation Company Limited, Beijing 102400, China
4   Graduate School, Daejin University, Pocheon-si 11159, Republic of Korea
*   Correspondence: yuliu@neepu.edu.cn

Abstract: Laser cladding is a new technology to improve the wear resistance or corrosion resistance properties of metal parts. A finite element model of laser cladding coating was established by numerical simulation technology. The temperature field distribution was studied and analyzed during the laser cladding process at three different scanning speeds and three different laser powers. A Ni-based coating was also fabricated on the substrate by a CO_2 laser. The optimum parameters of the laser cladding were selected and compared with the melt pool depth and width of the Ni-based coating. Then, the cooling rate, temperature gradient, temperature and stress fields were calculated and analyzed. The growth mechanism of the crystal structure was analyzed by scanning electron microscope (SEM). The wear resistance of the Ni-based coating was measured by a friction and wear testing machine. The results showed that the optimal parameters were laser power 1600 W and scanning speed 3 mm/s. The temperature trends at different locations were similar. The calculated maximum residual stress was 0.157 GPa. The stress concentration appeared near the surface and both sides of the cladding layer. From the coating's microstructure, it could be seen that it contained a large number of columnar dendrites, and the crystal size gradually decreased with the increase of cooling rate. The wear rates of the Ti-6Al-4V (TC4) substrate and the Ni-based coating were 6.98 mm^3/(N·m) and 3.45 mm^3/(N·m), respectively. The Ni-based layer had a low wear rate and good wear resistance, which is helpful to obtain good friction and wear resistance of TC4 substrates.

Keywords: laser cladding; numerical simulation; TC4 alloy; wear resistance

1. Introduction

Ti-6Al-4V (TC4) alloy parts have been used in the field of mechanical and metallurgical industries due to their excellent properties, such as low density and high specific strength [1,2]. However, TC4 alloy is often used in high-temperature and high-strength environments, making it prone to damage [3]. Surface modification technology can prepare coatings with excellent performance and prolong its service life. A lot of research has been carried out to improve the properties of titanium alloys, such as laser cladding technology, plasma arc welding technology and chemical physical vapor deposition technology. Laser cladding technology is used more and more due to its fast cooling rate, low coating dilution rate, easy operation, large temperature gradient and fine grain structure. During the process of laser cladding, the coating's quality can be affected by some factors, such as laser power, scanning speed and alloy composition [4,5]. In order to get a Ni-based coating with good properties, it is particularly important to obtain the accurate temperature and thermal stress. On one hand, because the process of laser cladding is complex and difficult to control, the temperature is difficult to measure accurately. Therefore, a numerical simulation method is usually used to study the thermal behavior of cladding coating. On the other

hand, the numerical simulation method is helpful to investigate the corresponding complex physical processes and reduce the experimental cost [6–8]. Therefore, some researchers have established some laser cladding models through numerical simulation techniques. The coating morphology was analyzed, and the best parameters were obtained [9,10].

The common laser cladding materials are mainly self-fluxing alloy powders, wherein Co-based, Ni-based and Fe-based self-fluxing alloy powders are the most widely used [11,12]. These three alloy powders have good wettability. The coating has low dilution and strong adhesion after laser cladding. These alloy powders are used to improve the performance of the parts [13,14]. Compared with Fe-based and Co-based powders, the outstanding advantages of Ni-based self-fluxing alloy powders are moderate price, good wear resistance, good wettability and sufficient raw materials [15].

Kumar Shakti et al. [16] used $Ti_6Al_4V:WS_2:Ni$ as a reinforcing material for laser cladding coating. The influence of different scanning speeds on the hardness, wear resistance and microstructure was discussed. Wang et al. [17] investigated the finite element simulation of TC4 alloy laser cladding under different laser powers and different scanning speeds. In the case of high laser power and low scanning speed, it was expected to form a good metallurgical bonding. Tian et al. [18] prepared an alloy coating on 304 stainless steel by laser cladding. The microstructure, size and stress field were investigated by numerical simulation. The microstructures in the coating were planar, honeycomb, dendrite and equiaxed crystals. Gao et al. [19] established a three-dimensional numerical single-channel model of laser cladding based on a Gaussian distribution heat source. The effect of different laser powers and different scanning speeds on the cladding geometry and temperature distribution was studied. The results showed that the height, width and molten pool temperature decreased along with the increase of scanning speed. When the height was stable, the width and molten pool temperature increased with the increase of laser power. Sun et al. [20] investigated a 3D Finite Element Method (FEM) for simulating the coating's temperature and stress fields. The experimental results showed that the high temperature and thermal gradient were generated near the heat source, which tended to generate residual stresses. The coating was prone to cracking in the vertical direction of the laser's moving direction. Guan et al. [21] used a Gaussian heat source to study the coating's temperature and the corresponding microstructure. The results showed that the temperature distribution coincided with the change of cooling rate around the cladding layer. Song et al. [22] melted $AlSi_{10}Mg$ powder on a 6061Al alloy substrate by laser. The residual stress and molten pool size were discussed. The residual stress increased with the increase of scanning speed and laser power. The residual tensile stress on both sides of the coating was high. Although there has been a lot of research about laser cladding simulation, there has been little research on the complex physical process involved in laser cladding coating on the surface of TC4 substrate by numerical simulation method.

In this research, the laser cladding process was simulated with the finite element model. A simulation model of laser cladding coating on TC4 substrate was established. Different laser parameters were selected to obtain the temperature field, which were used to investigate the morphology of the molten pool. The optimal parameters were selected. Then, the temperature and stress fields under the optimal parameters were calculated and analyzed. The characteristics of temperature change and stress distribution were expounded. The coating's cooling rate and temperature gradient were analyzed. The grain growth mechanism was revealed. Finally, the friction and wear resistance was investigated.

2. Experimental Materials and Methods

TC4 alloy was used as the substrate. The dimension was 50 × 30 × 10 mm. The surface of the TC4 alloy was finely ground before laser cladding and then cleaned with an alcohol sponge. The TC4 alloy composition is included in Table 1.

Table 1. Chemical composition of TC4 alloy substrate (wt.%).

Al	V	Fe	Si	C	Ti	N	O
6.01	3.84	0.30	0.15	0.10	89.3	0.15	0.15

The selected cladding material was a Ni-based alloy powder, with a size of 10–78 µm. The morphology is shown in Figure 1. The chemical composition of the Ni-based alloy powder is included in Table 2.
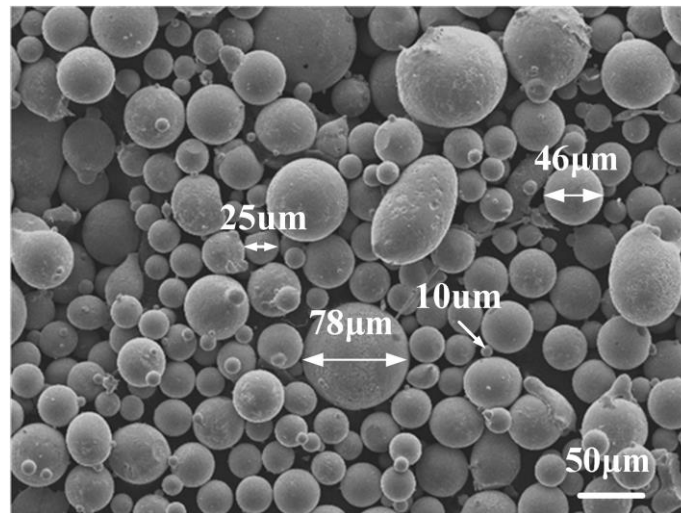
Figure 1. SEM micrograph of Ni-based alloy powder.

Table 2. Chemical composition of Ni-based alloy powder (wt.%).

C	B	Si	Cr	Fe	Ni
1.0	4.0	4.0	15.0	2.0	74.0

This experiment used a DL-HL-T2000 CO_2 laser. The thickness of alloy powder was about 1 mm on the surface of TC4 by preset powder method. The selected laser power was 1600 W. The scanning speed was 120 mm/min. The spot diameter was 3 mm. The distance between laser source and TC4 substrate surface was 330 mm. The overlapping ratio was 30%. Then, the coating was etched by an $HF:HNO_3:H_2O$ (1:2:17) etchant for 5 s. The microstructure was observed by SEM (Scanning Electron Microscope, ZEISS Gemini 300). The width and height of Ni-based coating were obtained with a 4XC-TV microscope. The friction and wear experiment was carried out by a reciprocating fatigue and wear tester (MGW-02). The frequency was 15 Hz. The load was 20 N. The friction and wear time was 20 min. The friction pair was GCr15 grinding ball with diameter of 6.5 mm.

3. Numerical Simulation of Laser Cladding

3.1. Establishment of Geometric Model

The TC4 alloy was used as the substrate. The coating thickness was set to 1 mm. Figure 2 shows the finite element model on the TC4 substrate. The grid is refined near the cladding layer. The transition grid technology was used to coarsen the regional grid away from the cladding layer to reduce the calculation cost and time. The 3D mesh refinement is shown in Figure 3.
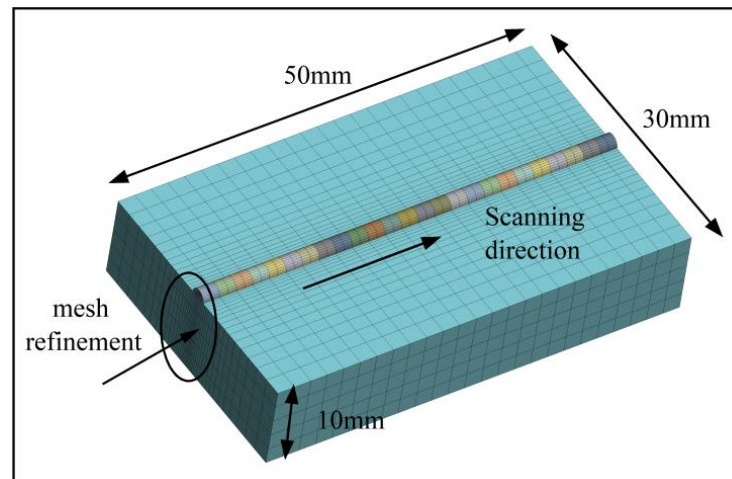
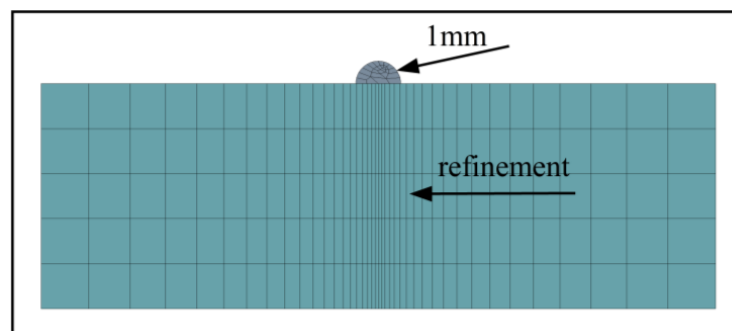**Figure 2.** Finite element model on the TC4 substrate.

Figure 3. Three-dimensional mesh refinement.

The mesh adopted a hexahedral element. The stretching method was used to divide the finite element mesh. For the improvement of the simulation accuracy, the birth-death element technology was used to establish a real-time filled cladding layer. The suppressed units were reactivated when they were affected by the heat source. Along with the laser spot scanning, the cladding layer was gradually activated to form a real-time filled cladding layer.

3.2. Material's Thermophysical Parameters

The JMatPro10.0 software was used to obtain the thermal physical and mechanical properties of cladding material and TC4, because the performance parameters of the material would change with the temperature during the laser cladding process. The thermal physical and mechanical properties are shown in Figures 4–6.

3.3. Boundary Conditions

The initial temperature of the laser cladding environment was set as 25 °C.

The heat loss of radiation was not considered. There was no heat transfer between the TC4 substrate and the test bench. The boundary conditions of each surface can be obtained by Equation (1):

$$-\lambda(T)\frac{\partial T}{\partial n} = h(T - T_0) \tag{1}$$

where $\lambda(T)$ is the thermal conductivity in W/(m·°C), T_0(=25 °C) is the environment temperature in °C, n is the normal vector on the selected surface and h is the convective heat transfer coefficient.
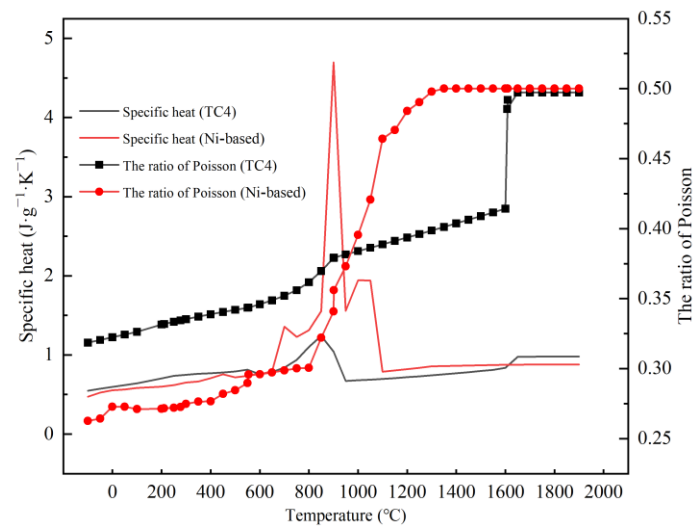
Figure 4. Material performance parameters: specific heat capacity and Poisson's ratio.
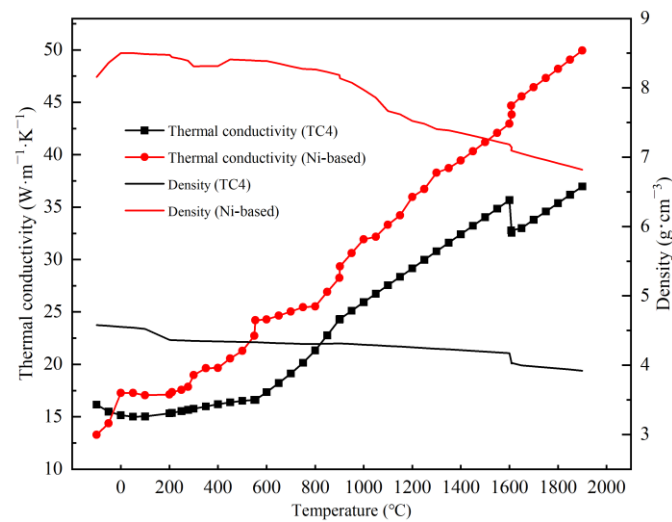

Figure 5. Material performance parameters: thermal conductivity and density.
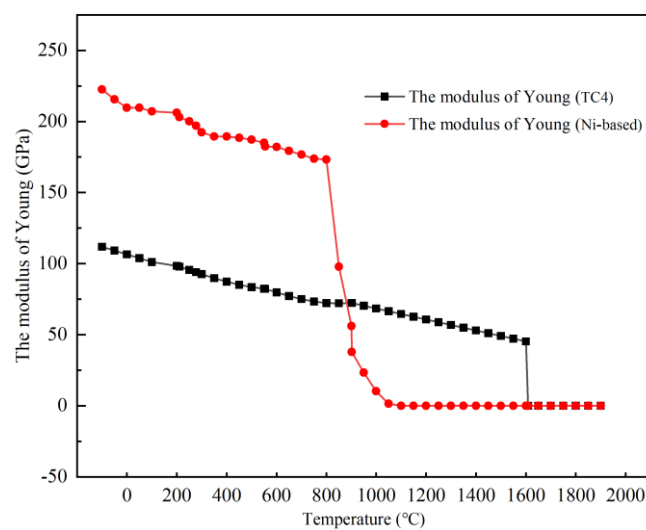

Figure 6. Material performance parameter: Young's modulus.

3.4. Heat Source Model

As the laser heat source, the Gaussian rotating body and double ellipsoid heat source are usually used. The position of the molten pool changes with the movement of the laser beam. It brings a significant difference to the morphology of the dynamic molten pool. When the beam is irradiated to the surface of Ni-based coating, the energy distribution inside the laser heat source spot becomes uneven. The energy in the center is more than the edge, and the energy is relatively concentrated in the center. Therefore, the Gaussian heat source model is used as the thermal load in this research.

The heat flux distribution function is as shown in Equation (2):

$$I(r) = (1 - R)\frac{2P}{\pi\omega^2}exp(-\frac{2r^2}{\omega^2}) \tag{2}$$

where R is the reflectivity, P is the laser power, ω is the spot radius and r is the transverse cylindrical coordinate.

3.5. Heat Conduction Control Equation

During the laser cladding process, there are some complex energy exchanges, such as heat transfer, convection and radiation. The temperature field of laser cladding is a typical nonlinear transient heat conduction problem, so the equation of transient temperature field can be simplified as Equation (3):

$$\rho c(T)\frac{\partial T}{\partial t} = \lambda(T)\left(\frac{\partial^2 T}{\partial x^2} + \frac{\partial^2 T}{\partial y^2} + \frac{\partial^2 T}{\partial z^2}\right) \tag{3}$$

where ρ is the density in kg/m^3, $c(T)$ is the specific heat in J/kg·°C, T is the temperature field distribution function during the experiment and $\lambda(t)$ is the thermal conductivity.

4. Analysis and Discussion

4.1. Temperature Field and Molten Pool Size Analysis

Figures 7–9 show the temperature field distribution during the laser cladding process at different laser powers and scanning speeds. The temperature fields of the molten pool have a gradient distribution. The temperature in the molten pool reaches the maximum value at the center point and gradually decreases from the center to the edge area. As shown in Figure 7a–c, when the laser power is 1500 W, the maximum temperatures at three different laser scanning speeds of 2, 3 and 4 mm/s are 3048.3, 2801.5 and 2684.1 °C in the coating's molten pool, respectively. If the laser power is the same, the maximum temperature gradually decreases with the increase of scanning speed. As shown in Figures 7a, 8a and 9a, when the laser scanning speed is 2 mm/s, the maximum temperatures at three different laser powers of 1500, 1600 and 1700 W are 3048.3, 3239.2 and 3514.7 °C in the coating's molten pool, respectively. If the scanning speed is the same, the maximum temperature gradually increases with the increase of laser power.
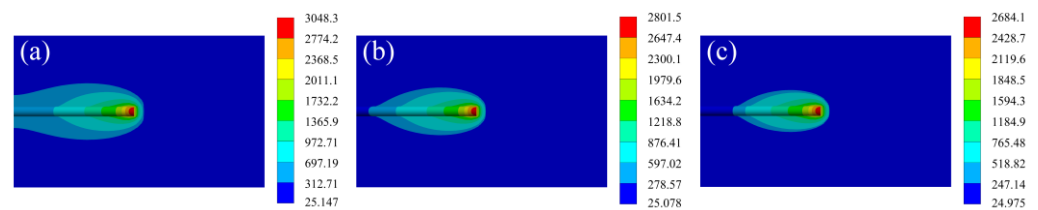

Figure 7. The temperature field distribution of the laser cladding process at laser power 1500 W with different scanning speeds. (**a**) 2 mm/s; (**b**) 3 mm/s; (**c**) 4 mm/s.
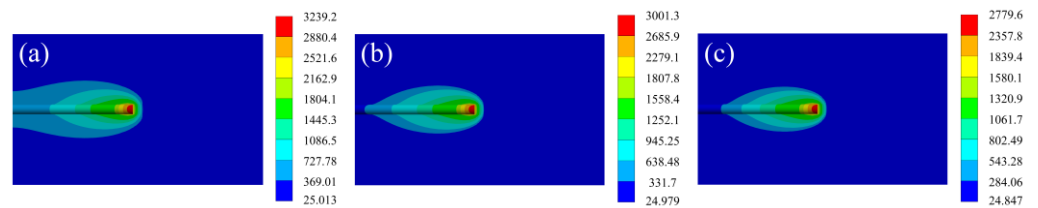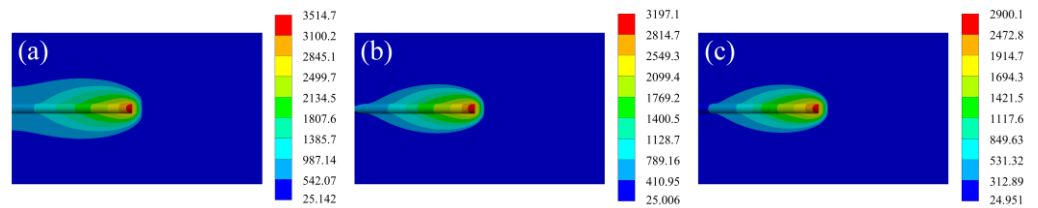
Figure 8. The temperature field distribution of the laser cladding process at laser power 1600 W with different scanning speeds. (**a**) 2 mm/s; (**b**) 3 mm/s; (**c**) 4 mm/s.

Figure 9. The temperature field distribution of the laser cladding process at laser power 1700 W with different scanning speeds. (**a**) 2 mm/s; (**b**) 3 mm/s; (**c**) 4 mm/s.

Figures 10–12 show the morphology of the molten pool at three different scanning speeds and three different laser powers. It can be seen that when the laser power is 1500 W, the depth and width of the coating's molten pool decrease with the increase of the laser scanning speed at the three different laser scanning speeds of 2, 3 and 4 mm/s. There is a similar trend in the laser power of 1600 and 1700 W. As shown in Figures 10a, 11a and 12a, when the scanning speed is 2 mm/s, the depth and width of the coating's molten pool increase with the increase of laser power. The scanning speeds of 3 and 4 mm/s obtain the same phenomenon. As shown in Figure 10, when the laser power is 1500 W, the depths of the molten pool at three different laser scanning speeds of 2, 3 and 4 mm/s are 1.03, 0.78 and 0.56 mm, respectively. As shown in Figure 11, when the laser power is 1600 W, the depths of the molten pool at three different laser scanning speeds of 2, 3 and 4 mm/s are 1.19, 0.87 and 0.62 mm, respectively. As shown in Figure 12, when the laser power is 1700 W, the depths of the molten pool at three different laser scanning speeds of 2, 3 and 4 mm/s are 1.34, 1.07 and 0.79 mm, respectively. When the depths of the coating's molten pool are 0.56 and 0.62 mm, the metallurgical bonding among the cladding layer and the substrate can be affected due to the small dilution rate. When the depth of the coating's molten pool is larger than 1 mm, a large dilution rate is generated, which damages some properties of the Ni-based cladding layer and increases the likelihood of cracks and deformation. Therefore, the optimum parameters can be obtained between 0.78, 0.79 and 0.87 mm. Due to the small difference in dilution rate, the large depth and width can obtain good bonding and performance between the Ni-based cladding layer and the TC4 substrate. Therefore, the coating of a depth of 0.87 mm and a width of 3.28 mm is supposed to obtain better performance. Therefore, the laser power of 1600 W and the laser scanning speed of 3 mm/s are used as the optimal laser parameters.
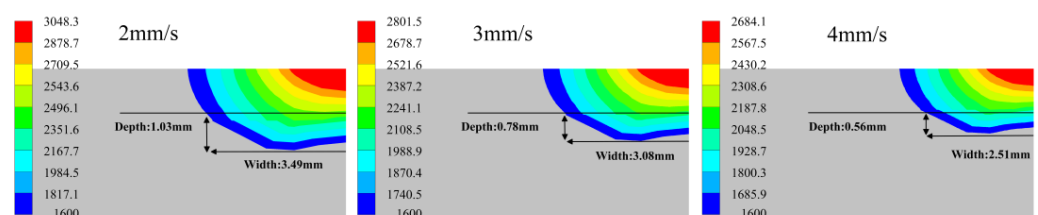

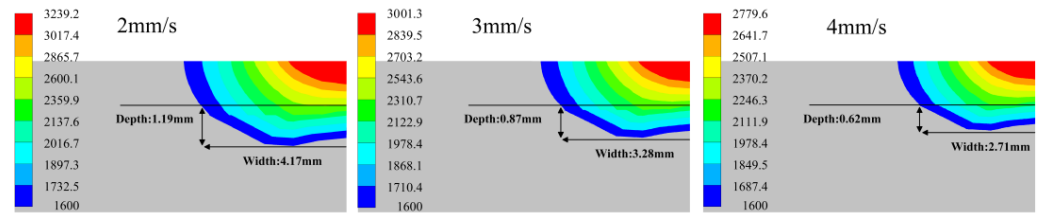**Figure 10.** Section morphology at laser power 1500 W at three different scanning speeds.

Figure 11. Section morphology at laser power 1600 W at three different scanning speeds.
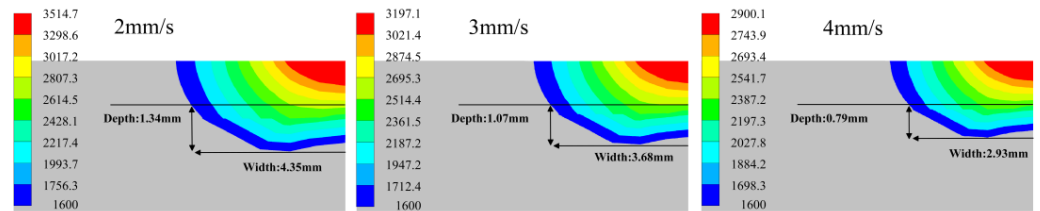

Figure 12. Section morphology at laser power 1700 W at three different scanning speeds.

Figure 13 shows the comparison between the simulated molten pool and the fabricated coating at laser power of 1600 W and laser scanning speed of 3 mm/s. Since the solidus temperature of TC4 alloy is 1600 °C, the simulated pool size can be obtained. The simulated pool depth is 0.87 mm and the width is 1.65 mm. The depth of the coating's molten pool calculated by experiment is 0.86 mm and the width is 1.64 mm. From the comparison of depth and width, the size of Ni-based coating is consistent with the simulated result.
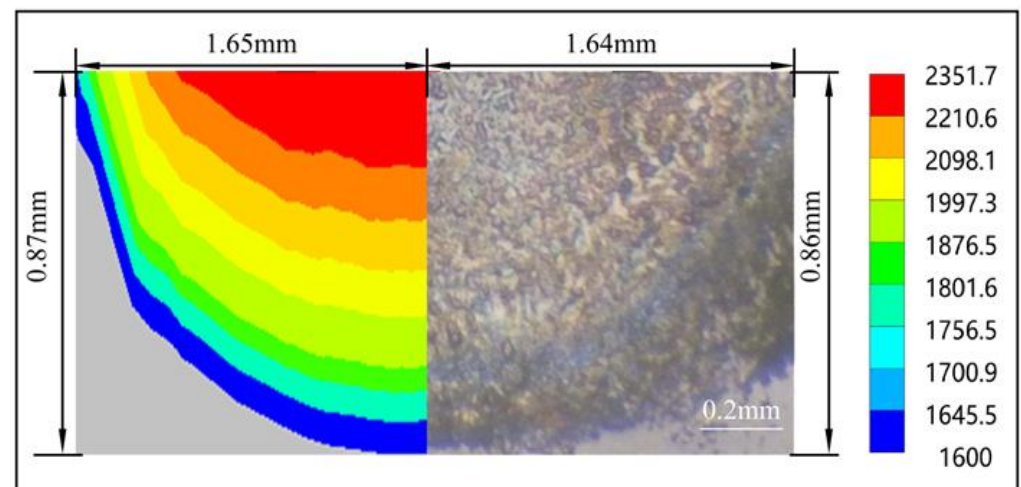

Figure 13. Comparison between the size of simulation of molten pool and experimental molten pool.

4.2. Temperature Cycle Characteristics

Some points A, B, C, D, E and F were selected to investigate the temperature field distribution at the same distances in the scanning direction, as shown in Figure 14.

Figure 15 shows the temperature change at different times in the horizontal direction. It can be seen that the temperature rises and falls of B~E points have similar trends. The maximum temperature of point A is 1967.8 °C. The maximum temperature of F point is 3168.5 °C. The reason is that the laser irradiation time is short at the beginning of laser cladding. With the accumulation of laser heat, the maximum temperature of the selected points increases. So, point F has a large amount of heat accumulation and the highest temperature.
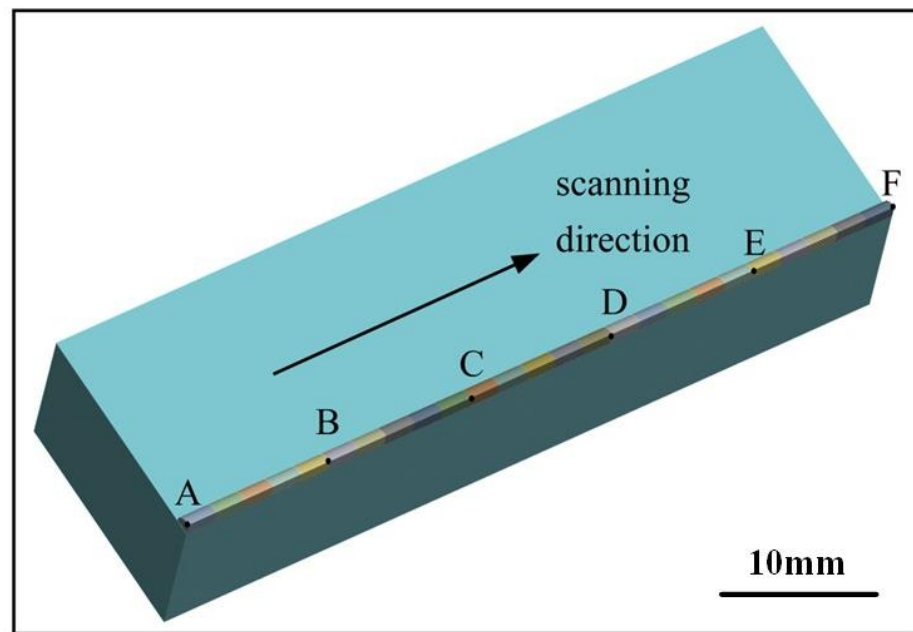
Figure 14. Horizontal direction path diagram on TC4 substrate: select points (A~F) at an interval of 10 mm.
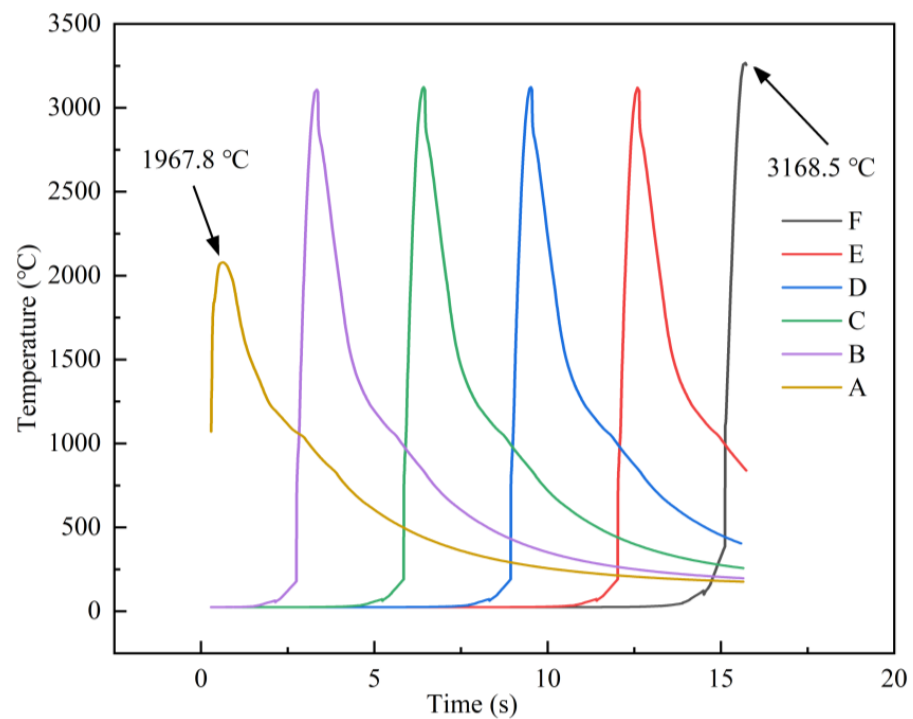

Figure 15. Temperature change at different times in the horizontal direction.

Figure 16 shows the longitudinal temperature when the laser cladding is carried out for 7 s. It can be seen that the temperature has a similar trend at different distances. The top position has the maximum temperature. The highest temperature in the laser molten pool can reach 3001.3 °C.
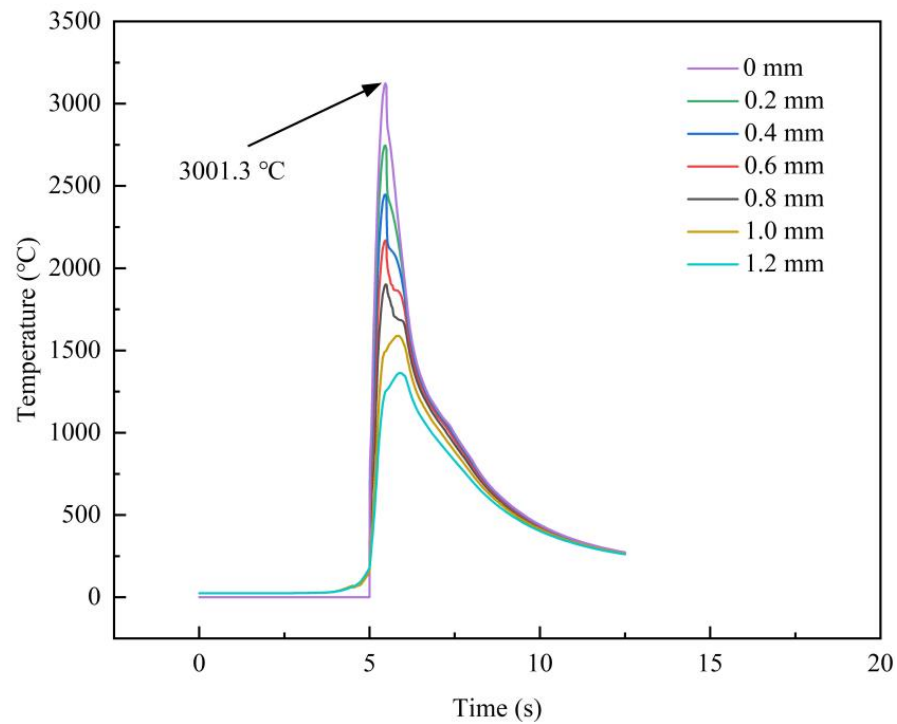
Figure 16. Temperature change at different times in the longitudinal direction.

Figure 17a–d show the temperature field clouds of points A, B, D and F in Figure 14. Some nodes near different positions are either heated or cooled during the laser cladding process. It leads to a large temperature gradient in the scanning direction. The molten material absorbs heat in a very short time, which makes the internal temperature increase drastically, while the molten layer can only dissipate heat through heat conduction and air convection.
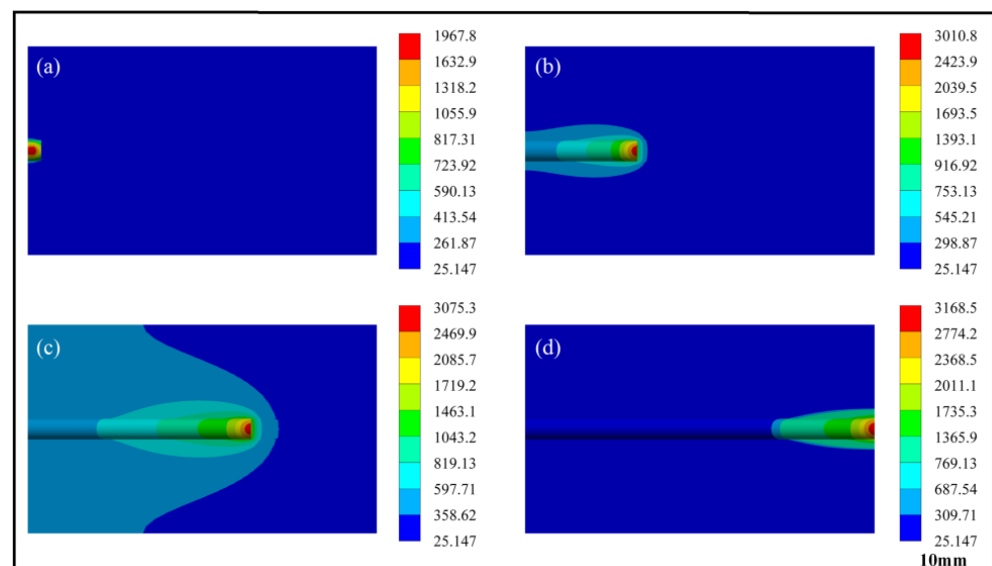

Figure 17. Temperature field clouds. (**a**) Point A; (**b**) Point B; (**c**) Point D; (**d**) Point F.

4.3. Stress Field Analysis

Figure 18 shows the residual stress field in the horizontal and vertical directions of the cladding layer. Figure 18a shows the residual stress field in the horizontal direction; it can be seen that the maximum residual stress appears near the surface of the Ni-based cladding layer and the edge area on both sides. The stress concentration phenomenon

is due to the high energy at the heat source's center and the low energy at the periphery. Figure 18b shows the residual stress field in the vertical direction; the stress is larger around the bonding zone between the Ni-based cladding layer and the TC4 substrate. This is caused by the different properties of the Ni-based cladding material and TC4 substrate, which cause stress concentration. Therefore, there is a maximum residual stress around the bonding zone between the Ni-based coating and the TC4 substrate.
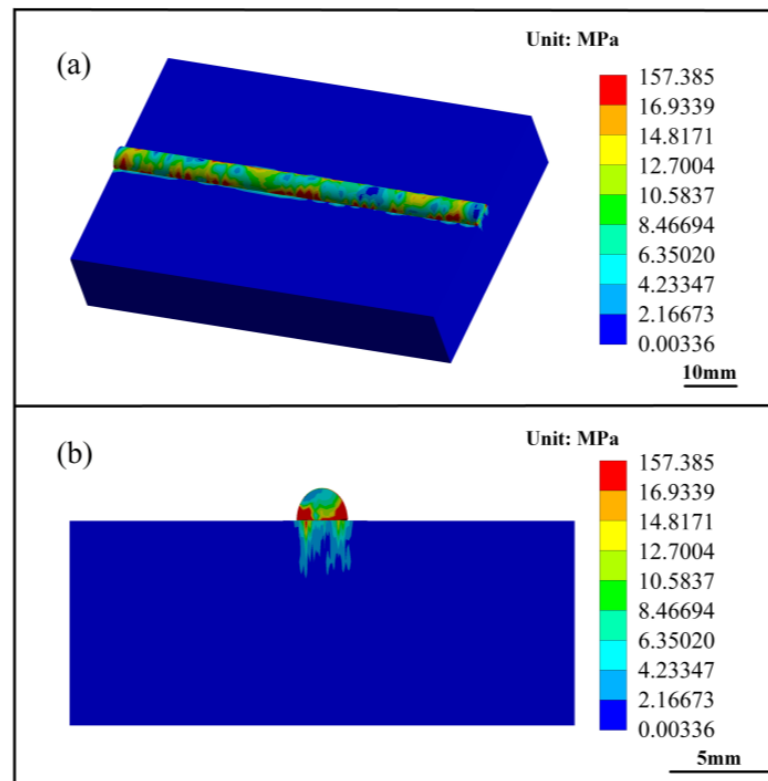

Figure 18. Residual stress field in different directions: (**a**) horizontal direction; (**b**) vertical direction.

4.4. Temperature Gradient, Cooling Rate and Microstructure Analysis

From the previous study, cooling rate and temperature gradient were the key parameters to the coating's quality. As can be seen in Figure 19, it shows the variation of temperature gradient and cooling rate at different positions from the Ni-based cladding layer to the bottom in the molten pool. The maximum temperature gradient is 1285.9 °C/mm near the top of the Ni-based cladding layer. The minimum temperature gradient is 710.9 °C/mm. The temperature gradient shows a fast-slow-fast-slow trend from the top of the Ni-based cladding layer to the bottom of the molten pool. The reason is that the difference of temperature is too large between the unheated area and the surface of the Ni-based cladding layer. There is a large cooling rate near the top of the cladding layer. The values of maximum and minimum cooling rates are 1723.3 and 372.2 °C/s. The cooling rate decreases with the increase of distance from the top of the Ni-based cladding layer.

Figure 20 shows the microstructures in regions A and B at the bottom of the Ni-based coating. As can be seen in Figure 20, some columnar dendrites appear at the bottom of the coating's molten pool. Due to the negative correlation between the growth of crystals' grain size and the cooling rate of the molten pool, the grain size decreases when the cooling rate becomes large. While the cooling rate is relatively small, the grains have enough time to grow. So, the size in region B is relatively large. In front of region B, the grain size becomes smaller at region A.
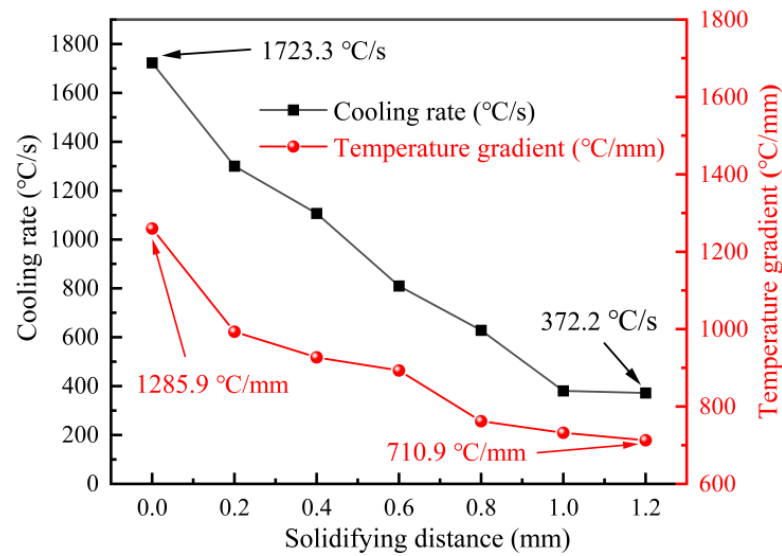
Figure 19. Temperature gradient and cooling rate from the top of the cladding layer to the bottom of the molten pool.
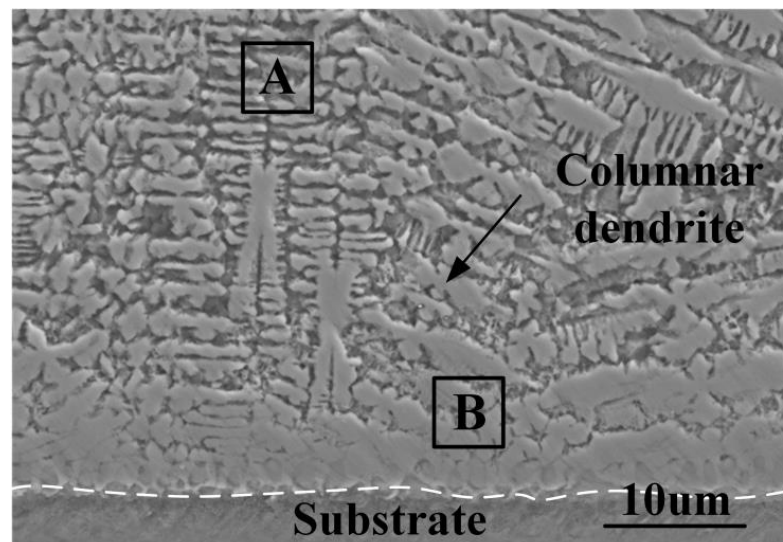

Figure 20. Microstructure of Ni-based coating in regions A and B at the bottom of the Ni-based coating.

4.5. Friction and Wear Resistance

Figure 21 shows the friction coefficient curve of the TC4 substrate and Ni-based coating. In Figure 21a, the friction coefficient of the TC4 substrate increases rapidly at the beginning of the friction and wear experiment. It gradually stabilizes at about 0.4 after a few minutes. In Figure 21b, the change of the coating's friction coefficient has a small fluctuation at the beginning of the friction and wear experiment. The maximum value is 0.38 at 150 s, which gradually stabilizes at about 0.3. Figure 22 shows the average friction coefficient of the TC4 substrate and Ni-based coating; it can be seen that the average friction coefficient of the Ni-based coating is smaller than the TC4 substrate.
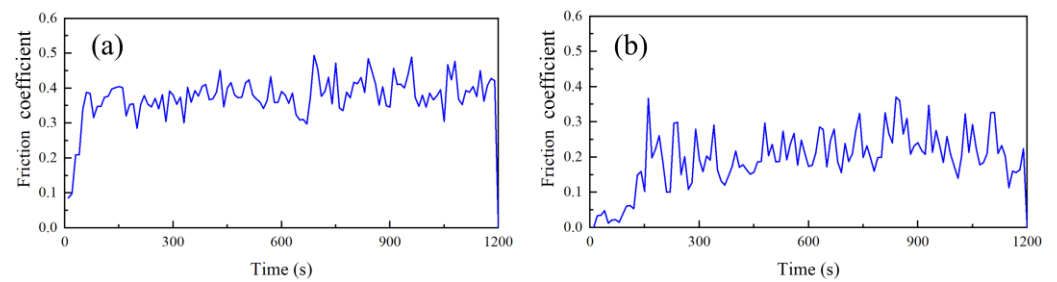
Figure 21. Friction coefficient: (**a**) TC4 substrate; (**b**) Ni-based coating.
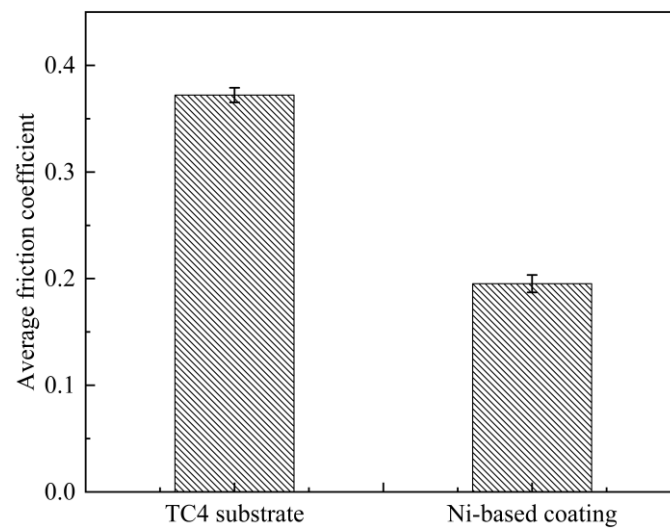

Figure 22. Average friction coefficient of TC4 substrate and Ni-based coating.

As can be seen in Figure 23, the wear rates of the TC4 substrate and Ni-based coating are 6.98 mm^3/(N·m) and 3.45 mm^3/(N·m), respectively. The wear rate of the TC4 substrate is about twice that of the Ni-based coating, indicating that the Ni-based coating is helpful to increase the wear resistance of the TC4 substrate.
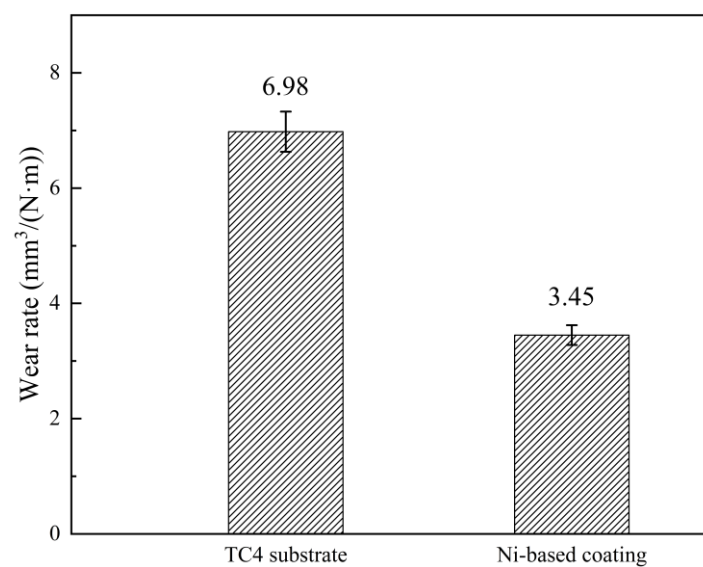

Figure 23. Wear rates of TC4 substrate and Ni-based coating.

5. Conclusions

(1) A three-dimensional mesh model of Ni-based cladding coating was established on TC4 substrate. The temperature field under three different laser scanning speeds was calculated. The optimal parameters obtained were as follows: laser power 1600 W and scanning speed 3 mm/s. By comparing the depth and width of the coating's molten pool, the result of numerical simulation was in accordance with the fabricated coating.

(2) The thermal cycling simulation of cladding coating in the horizontal and vertical directions was investigated at laser power of 1600 W and scanning speed of 3 mm/s. In the horizontal direction, the temperature of point A was 1967.8 °C due to the short time of laser irradiation. Point F had the highest temperature of 3168.5 °C due to unidirectional heat conduction. The temperature change trend of points B~E was similar. In the vertical position from the surface to the bottom of the cladding coating, the temperature change trend at different positions was basically the same. The highest temperature of the cladding coating was 3001.3 °C. The stress concentration mainly appeared on the top of the Ni-based cladding layer, near the TC4 substrate area on two sides and the Ni-based coating bonding area. The maximum value of residual stress was 0.157 GPa.

(3) Columnar dendrites appeared at the bottom of the coating's molten pool. Due to the negative correlation between the growth of grain size and the cooling rate, the grain size gradually decreases when the cooling rate increases. If the cooling rate is relatively small, the grains have enough time to grow. The grain size in region B was large. The wear rates of the TC4 substrate and the Ni-based coating were 6.98 $mm^3/(N\cdot m)$ and 3.45 $mm^3/(N\cdot m)$. The Ni-based coating is helpful to reduce the wear rate of the TC4 substrate and obtain a good friction and wear resistance.

Author Contributions: Software, Y.L.; writing-original draft, X.L.; resources, Y.L.; data processing, X.L.; investigation, Z.X.; formal analysis, M.Y.; supervision, Y.L. and M.Y. All authors have read and agreed to the published version of the manuscript.

References

1. Pang, X.T.; Yao, C.W.; Xiong, Z.H.; Gong, Q.F.; Sun, J.H.; Misra, R.D.K.; Li, Z.G. Comparative study of coatings with different molybdenum equivalent on titanium alloy forged plate for laser cladding: Microstructure and mechanical properties. *Surf. Coat. Technol.* **2022**, *446*, 128760. [CrossRef]
2. Yang, X.Y.; Wang, L.L.; Gao, Z.N.; Wang, Q.; Du, M.Z.; Zhan, X.H. WC distribution, microstructure evolution mechanism and microhardness of a developed Ti-6Al-4V/WC MMC coating fabricated by laser cladding. *Opt. Laser Technol.* **2022**, *153*, 108232. [CrossRef]
3. Zhang, K.M.; Zou, Z.X.; Li, J.; Yu, Z.S.; Wang, H.P. Surface modification of TC4 Ti alloy by laser cladding with TiC+Ti powders. *Trans. Nonferr. Met. Soc. China* **2010**, *20*, 2192–2197. [CrossRef]
4. Youssef, D.; Hassab-Elnaby, S.; Al-Sayed, S.R. New 3D model for accurate prediction of thermal and microstructure evolution of laser powder cladding of Ti$_6$Al$_4$V alloy. *Alex. Eng. J.* **2022**, *61*, 4137–4158. [CrossRef]
5. Zhu, L.D.; Xue, P.S.; Lan, Q.; Meng, G.R.; Ren, Y.; Yang, Z.C.; Xu, P.H.; Liu, Z. Recent research and development status of laser cladding: A review. *Opt. Laser Technol.* **2021**, *138*, 106915. [CrossRef]
6. Florian, W.; Konrad, W. A physical modeling and predictive simulation of the laser cladding process. *Addit. Manuf.* **2018**, *22*, 307–319.
7. Lu, X.F.; Lin, X.; Michele, C.; Miguel, C.; Li, J.J.; Ma, L.; Wei, L.; Hu, Y.L.; Huang, W.D. Finite element analysis and experimental validation of the thermomechanical behavior in laser solid forming of Ti-6Al-4V. *Addit. Manuf.* **2018**, *21*, 30–40. [CrossRef]

8. Nusrat, T.; Roger, C.; Sumsun, N. Progress in numerical simulation of the laser cladding process. *Opt. Lasers Eng.* **2019**, *122*, 151–163.

9. Liu, Y.D.; Zhou, Y.S.; Shi, W.T.; Han, J.; Ye, D.L.; Han, Y.F. Experimental research on variable parameter forming process for forming specimen of TC4 titanium alloy by selective laser melting. *Materials* **2022**, *15*, 6408. [CrossRef]

10. Wang, C.Y.; Zhou, J.Z.; Zhang, T.; Meng, X.K.; Li, P.F.; Huang, S. Numerical simulation and solidification characteristics for laser cladding of Inconel 718. *Opt. Laser Technol.* **2022**, *149*, 107843. [CrossRef]

11. Zeng, M.; Yan, H.; Yu, B.B.; Hu, Z. Microstructure, microhardness and corrosion resistance of laser cladding Ni–WC coating on AlSi5Cu1Mg alloy. *Trans. Nonferr. Met. Soc. China* **2021**, *31*, 2716–2728. [CrossRef]

12. Wang, Q.; Li, Q.; Zhang, L.; Chen, D.X.; Jin, H.; Li, J.D.; Zhang, J.W.; Ban, C.Y. Microstructure and properties of Ni-WC gradient composite coating prepared by laser cladding. *Ceram. Int.* **2022**, *48*, 7905–7917. [CrossRef]

13. Farahmand, P.; Kovacevic, R. Corrosion and wear behavior of laser cladded Ni–WC coatings. *Surf. Coat. Technol.* **2015**, *276*, 121–135. [CrossRef]

14. Liu, Y.; Li, Z.; Li, G.; Du, F.; Yu, M. Microstructure and wear resistance of Ni-WC-TiC alloy coating fabricated by laser. *Lubricants* **2023**, *11*, 170. [CrossRef]

15. Yu, Q.; Wang, C.; Zhao, Z.; Dong, C.; Zhang, Y. New Ni-based superalloys designed for laser additive manufacturing. *J. Alloys Compd.* **2021**, *861*, 157979. [CrossRef]

16. Kumar, S.; Kumar, M.; Mandal, A.; Das, A. Ni-WS$_2$-Ti-6Al-4V self-lubricating coating on TC4 alloy by laser cladding. *Surf. Eng.* **2022**, *38*, 313–323. [CrossRef]

17. Wang, C.; Deng, C.; Wu, Y.R.; Chai, L.J.; Xiang, K.; Huang, Y. Temperature and stress field analysis for pulsed laser-cladding of pure titanium on Ti-6Al-4V. *JOM* **2022**, *74*, 755–763. [CrossRef]

18. Tian, J.Y.; Xu, P.; Chen, J.H.; Liu, Q.B. Microstructure and phase transformation behaviour of a Fe/Mn/Si/Cr/Ni alloy coating by laser cladding. *Opt. Lasers Eng.* **2019**, *122*, 97–104. [CrossRef]

19. Gao, J.L.; Wu, C.Z.; Hao, Y.B.; Xu, X.C.; Guo, L.J. Numerical simulation and experimental investigation on three-dimensional modelling of single-track geometry and temperature evolution by laser cladding. *Opt. Laser Technol.* **2020**, *129*, 106287. [CrossRef]

20. Sun, S.T.; Fu, H.G.; Chen, S.Y.; Ping, X.L.; Wang, K.M.; Guo, X.Y.; Lin, J.; Lei, Y.P. A numerical-experimental investigation of heat distribution, stress field and crack susceptibility in Ni60A coatings. *Opt. Laser Technol.* **2019**, *117*, 175–185. [CrossRef]

21. Srinivasan, A.; Li, Y.H.; Nie, L.; Guan, Y.C.; Yang, S.F. Microstructural evolution and properties analysis of laser surface melted and Al/SiC cladded magnesium-rare earth alloys. *J. Alloys Compd.* **2020**, *848*, 156598.

22. Song, C.Y.; Wang, W.Y.; Ren, Z.Q.; Zhao, Y.; Zhou, L. Numerical and experimental study on the properties of laser cladding of 6061Al alloy. *Trans. Indian Inst. Met.* **2022**, *75*, 1355–1364. [CrossRef]